Ground Target Tracking Using Terrain Information

Adam M. Fosbury
Dept. of Mech. & Aero. Eng.
University at Buffalo
Amherst, NY 14260-4400
amfosbury@yahoo.com

John L. Crassidis
Dept. of Mech. & Aero. Eng.
University at Buffalo
Amherst, NY 14260-4400
johnc@eng.buffalo.edu

Tarunraj Singh
Dept. of Mech & Aero. Eng.
University at Buffalo
Amherst, NY 14260-4400
tsingh@eng.buffalo.edu

Clyde Springen
Fusion Technology Group
Overwatch Systems
West Lake Hills, TX 78746
clyde.springen@overwatch.com

Abstract - ***In this paper a hybrid Kalman filter is derived for the tracking of ground based targets. The propagation is performed using unscented Kalman filter equations, while the updates are performed using extended Kalman filter equations. The novel feature of this hybrid filter is that terrain information has been incorporated to improve the accuracy of state estimates. This information, termed trafficability, incorporates local terrain slope, ground vegetation and other factors to put constraints on the vehicles maximum speed. The estimated velocity vector is deflected based on the trafficability values of nearby locations. Simulations show that the use of trafficability can improve estimated accuracy in locations where the vehicle path is influenced by terrain features.***

Keywords: trafficability, filtering, extended Kalman filter, unscented Kalman filter, target tracking.

1 Introduction

Roads are the primary terrain feature in most target tracking studies. Vehicles traveling on a road are often assumed to remain on the road. Those that are traveling off-road but come within a certain proximity are expected to seek entrance to the road. The benefit of a vehicle traveling on a road is that the geometric shape of the road becomes a constraint to the two-dimensional target tracking problem. This reduces it to a single dimension tracking problem. They are characterized by several different factors, including type, location, surface material and surface quality. Varying elevation is another important factor in target tracking. Vehicles climbing an incline will generally do so with reduced speed. If the incline is too steep, some vehicles will be unable to move through that area. Conversely, a vehicle traveling down an incline will move at a greater speed than normal.

For off-road travel, the type of terrain is necessary knowledge. Forests can have varying densities with some allowing large vehicles through, and others preventing everything except people from traversing. A road passing through a forest acts somewhat like a tunnel, keeping the vehicle from leaving the road at any point. Non-shallow bodies of water will be impassable for most vehicles. Swamps and wetlands will also place constraints on the types of vehicles that can travel through them. Canyons and cliffs will act as barriers to vehicle travel. An open level plain is the most unconstrained terrain that is likely to be encountered.

Several approaches can be used for robust tracking of vehicles. Kastella and Kreucher [1] use real data of battle simulations for its tests. A description of the terrain was not provided, but it is assumed to be non-road based. Layne and Piyasena [7] simulate a single target maneuvering in the X-Y plane with no terrain features. Yan et al. [8] use a continuous path of three straight line segments separated by constant turn rate maneuvers. Kim and Lee [26] simulate a target with varying velocity, sinusoidal acceleration, and coordinated turning. Enders [21] looks at road target tracking. Trajectories consist of consecutive straight line segments where intersections are hard angles. A combination of on and off road terrain is used by Reid and Bryson [27]. The exact makeup of the terrain is not provided, though it is modeled by a potential field approach. Payne and Marrs [13] examine a four-road network that is broken up into six segments. The four roads intersect each other at the same location. A grid-style road network is simulated by Hernandez [14]. It is described as a Manhattan style network, where all roads form a grid of square cells. At each intersection, a probability is defined to indicate whether the vehicle

Table 1: Comparison of Reviewed Literature For Single Target Tracking Algorithms

Ref. #	[1], [2], [3] [4], [5], [6]	[7], [8], [9] [10], [11], [12]	[13], [14], [15], [16] [17], [18], [19], [20]	[21], [22], [23] [24], [25]
Approach	MM	A-IMM	VS-IMM	Other
Data Type	GPS, Radar	–	GMTI	GMTI
System Hypotheses	Vertical Acceleration NCV Circular Motion Constant Acceleration Wiener Acceleration	Constant Acceleration NCV Constant Turn Rate	NCV Move-Stop-Move	NCV
Terrain	Road, None, Off-Road	None	Road, Off-Road	Road, None, Off-Road

will continue straight, or make a turn. Arulampalam et al. [15] study a simple three-road network, where all roads converge at the same point. Cheng and Singh [16] simulate a continuous three road network. The first turn is acute, while the second turn is ninety degrees.

Hernandez [14] derives the Posterior Cramér-Rao Lower Bound (PCRLB) for tracking road-based vehicles using Ground Moving Target Indicator (GMTI) sensors. This poses a challenging problem the structure of the road network must be accounted for, as well as the concurrent constrained applied with it. Since an analytical solution for the PCRLB is intractable, the bound is instead computed via Monte Carlo simulation. However, because problems associated with multi-modality of the target distribution at each junction, the resulting computed PCRLB may be over-optimistic. Hence, an alternative performance measure (APM) is introduced that resembles the error covariance of an extended Kalman filter with measurements linearized around the true target state and known target maneuvers. The assumed measurements are bearing, range and range-rate. Simulation results are provided using a Manhattan road network in two-dimensional space. A variable structure, multiple model particle filter (VS-MM-PF) is used to rest the performance of the Monte Carlo based PCRLB solution and the APM. The PCRLB is shown to be hugely over-optimistic, while the APM is shown to accurately predict the performance of the VS-MM-PF. Table 1 provides a summary and comparison of various algorithms for ground tracking of vehicles, involving Multiple Model (MM), Adaptive Interacting Multiple Model (A-IMM), Variable Structure Interacting Multiple Model (VS-IMM) and other approaches. All of these approaches are based on a near constant velocity model (NCV) in some form.

This paper looks to examine the use of terrain information in the estimation of a ground vehicle's position. Terrain slope and other data is used to generate trafficability values between 0 and 1, corresponding to the percentage of maximum velocity that a vehicle can achieve at that particular location. The estimated velocity vector is then deflected based upon the trafficability in the local region. A hybrid filter is used combining the update steps of the extended Kalman filter with the propagation steps of the unscented Kalman filter.

2 Reference Frames

This section summarizes the various reference frames used in the remainder of this paper, as shown in Fig. 1:

- Earth-Centered-Inertial (ECI): denoted by $\{\hat{\mathbf{i}}_1, \hat{\mathbf{i}}_2, \hat{\mathbf{i}}_3\}$. The origin is at the center of the Earth, with the $\hat{\mathbf{i}}_1$ axis pointing in the direction of the vernal equinox, the $\hat{\mathbf{i}}_3$ axis pointing towards the North pole, while $\hat{\mathbf{i}}_2$ completes the right-handed coordinate system. This frame is fixed in space, with associated vectors identified by the letter I.

- Earth-Centered-Earth-Fixed (ECEF): denoted by $\{\hat{\mathbf{e}}_1, \hat{\mathbf{e}}_2, \hat{\mathbf{e}}_3\}$. The origin of this frame is also located at the center of the Earth. The primary difference is that this frame rotates with the Earth. The $\hat{\mathbf{e}}_3$ axis points towards the north pole and is equal to $\hat{\mathbf{i}}_3$. The $\hat{\mathbf{e}}_1$ axis is directed toward the prime meridian, and the $\hat{\mathbf{e}}_2$ axis completes the right-handed system. The

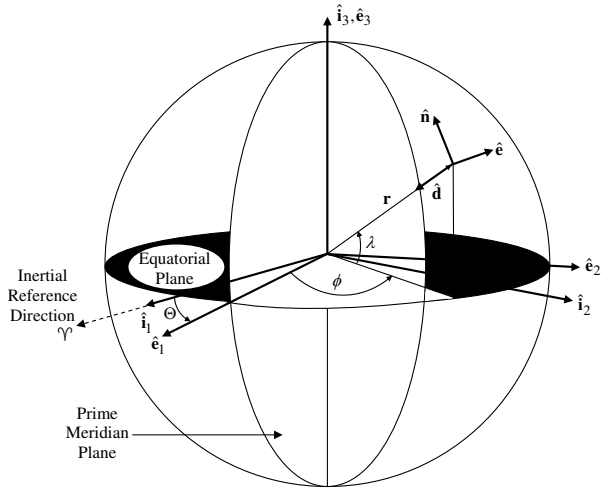

Figure 1: Definitions of Various Reference Frames

letter E signifies a vector defined with respect to this reference frame.

- North-East-Down (NED): denoted by $\{\hat{\mathbf{n}}, \hat{\mathbf{e}}, \hat{\mathbf{d}}\}$. This reference frame is formed by fitting a tangent plane to the geodetic reference ellipse at a given point of interest [28]. The $\hat{\mathbf{n}}$ axis points North, the $\hat{\mathbf{e}}$ axis is directed East, and the $\hat{\mathbf{d}}$ axis completes the right-handed system. This reference frame is generally used for local navigation purposes. The letter N signifies a vector defined with respect to this reference frame.

The convention applied in this paper is to use these letters as a superscript following the vector or matrix that is being described.

An overview of the conversion between the ECEF and NED reference frames is provided here. For a more complete discussion, see Ref. [28]. Given the latitude (λ), longitude (ϕ), and height (h), the ECEF coordinates are given by the equations

$$\mathbf{r}^E \equiv \begin{bmatrix} r_1^E \\ r_2^E \\ r_3^E \end{bmatrix} = \begin{bmatrix} (N+h)\cos\lambda\cos\phi \\ (N+h)\cos\lambda\sin\phi \\ \left[N(1-e^2)+h\right]\sin\lambda \end{bmatrix} \quad (1)$$

where $e = 0.0818$ is the eccentricity of the Earth's ellipsoid using a WGS-84 ellipsoid model, and N is the length of the normal to the ellipsoid given by the equation

$$N = \frac{a}{\sqrt{1-e^2\sin^2\lambda}} \quad (2)$$

where a is the semimajor axis of the ellipsoid and is equal to 6,378,137 meters. Conversion from ECEF position to latitude and longitude is more difficult. A complicated closed form solution is given in Ref. [28]. However, a good approximation up to low Earth orbit is provided by Ref. [29]:

$$p = \sqrt{(r_1^E)^2 + (r_2^E)^2} \quad (3a)$$

$$\zeta = \text{atan}\left(\frac{r_3^E\, a}{p\, b}\right) \quad (3b)$$

$$\bar{e}^2 = \frac{a^2-b^2}{b^2} \quad (3c)$$

$$\lambda = \text{atan}\left(\frac{r_3^E + \bar{e}^2\, b\, \sin^3\zeta}{p - e^2\, a\, \cos^3\zeta}\right) \quad (3d)$$

$$\phi = \text{atan2}(r_2^E,\, r_1^E) \quad (3e)$$

$$h = \frac{p}{\cos\lambda} - N \quad (3f)$$

where $b = 6356752.3142$ meters is the semiminor axis. The height (h) will be determined from a database that contains elevation values for a given latitude and longitude.

The direction cosine matrix relating the NED and ECEF reference frames is given in Ref. [28]:

$$A_E^N = \begin{bmatrix} -\sin\lambda\cos\phi & -\sin\lambda\sin\phi & \cos\lambda \\ -\sin\phi & \cos\phi & 0 \\ -\cos\lambda\cos\phi & -\cos\lambda\sin\phi & -\sin\lambda \end{bmatrix} \quad (4)$$

The NED position with a reference frame originating at latitude λ_0, longitude ϕ_0 and height h_0 is given by

$$\mathbf{r}^N = A_E^N(\lambda_0, \phi_0, h_0)(\mathbf{r}^E - \mathbf{r}_0^E) \quad (5)$$

where $\mathbf{r}^E$ and $\mathbf{r}_0^E$ are given by Eq. (1) with the latter being a function of the NED coordinates at the origin of the reference frame.

3 Filter

The state vector used in the filter is given by

$$\mathbf{x} = \begin{bmatrix} \lambda & \phi & v_n & v_e \end{bmatrix}^T \quad (6)$$

where v_n and v_e are the northward and eastward velocities given in an NED reference frame. The standard "$\alpha - \beta$" tracker approach assumes a first-order random-walk process for the accelerations [30]. Our approach modifies this concept by using the following model:

$$\mathbf{x}_{k+1} = \left.\begin{bmatrix} \lambda + \dfrac{v_n \Delta t}{R_\lambda + h} \\ \phi + \dfrac{v_e \Delta t}{(R_\phi + h)\cos\lambda} \\ \nu\sqrt{v_n^2 + v_e^2}\cos\theta \\ \nu\sqrt{v_n^2 + v_e^2}\sin\theta \end{bmatrix}\right|_k + \mathbf{w}_k \quad (7)$$

where R_λ and R_ϕ are defined in Ref. [28] as

$$R_\lambda = \frac{a(1-e^2)}{(1-e^2\sin^2\lambda)^{3/2}} \quad (8)$$

$$R_\phi = \frac{a}{(1-e^2\sin^2\lambda)^{1/2}} \quad (9)$$

and

$$E\{\mathbf{w}_k\mathbf{w}_k^T\} = \Delta t \Upsilon \begin{bmatrix} q_x & 0 \\ 0 & q_y \end{bmatrix} \Upsilon^T \quad (10)$$

with

$$\Upsilon \equiv \begin{bmatrix} 0 & 0 \\ 0 & 0 \\ 1 & 0 \\ 0 & 1 \end{bmatrix} \quad (11)$$

The angle θ, which is the angle between the velocity vector and the local x-axis, defines the assumed direction of motion of the vehicle. This is determined by use of the trafficability matrix. The coefficient ν is a number between zero and one that defines the velocity constraint in that region. This will be explained further in the next section. The $\sqrt{v_n^2 + v_e^2}$ term is simply the magnitude of the vehicle velocity. The trigonometric terms are used to project this value onto the North and East axes. When no terrain information is present, ν defaults to one, and the trigonometric terms are given by

$$\cos\theta = \frac{v_n}{\sqrt{v_n^2 + v_e^2}} \quad (12)$$

$$\sin\theta = \frac{v_e}{\sqrt{v_n^2 + v_e^2}} \quad (13)$$

which reduces to the standard $\alpha - \beta$ form. Note that the first two states of Eq. (7) represent a simple first-order discrete-time propagation of the kinematic models, which is valid for small Δt. A higher-order integration can be employed if needed.

The filter model in Eq. (7) represents a highly nonlinear model. Specifically, as will be shown later, the variable θ is a function of the filter states. The EKF requires taking partial derivatives of the model for the state and covariance propagation, which is intractable due to θ. Hence, a hybrid UF/EKF is chosen for the filter design. The EKF is used for the update state, given by the following equations [30]:

$$K_k = P_k^- H_k^T(\hat{\mathbf{x}}_k^-)[H_k(\hat{\mathbf{x}}_k^-)P_k^- H_k^T(\hat{\mathbf{x}}_k^-) + R_k]^{-1} \quad (14a)$$

$$\hat{\mathbf{x}}_k^+ = \hat{\mathbf{x}}_k^- + K_k[\tilde{\mathbf{y}}_k - \mathbf{h}(\hat{\mathbf{x}}_k^-)] \quad (14b)$$

$$P_k^+ = [I - K_k H_k(\hat{\mathbf{x}}_k^-)]P_k^- \quad (14c)$$

The UF is used for the propagation stage, given by the following equations [31]:

$$\boldsymbol{\sigma}_k \leftarrow 2n \text{ columns from } \pm\gamma\sqrt{P_k^+ + \Upsilon_k Q_k \Upsilon_k^T} \quad (15a)$$

$$\boldsymbol{\chi}_k(0) = \hat{\mathbf{x}}_k^+ \quad (15b)$$

$$\boldsymbol{\chi}_k(i) = \boldsymbol{\sigma}_k(i) + \hat{\mathbf{x}}_k^+ \quad (15c)$$

and

$$\boldsymbol{\chi}_{k+1}(i) = \mathbf{f}(\boldsymbol{\chi}_k(i),\, \mathbf{u}_k,\, k) \quad (16a)$$

$$\hat{\mathbf{x}}_{k+1}^- = \sum_{i=0}^{2n} W_i^{\text{mean}}\, \boldsymbol{\chi}_{k+1}(i) \quad (16b)$$

$$P_{k+1}^- = \sum_{i=0}^{2n} W_i^{\text{cov}}\, [\boldsymbol{\chi}_{k+1}(i) - \hat{\mathbf{x}}_{k+1}^-]\, [\boldsymbol{\chi}_{k+1}(i) - \hat{\mathbf{x}}_{k+1}^-]^T \quad (16c)$$

The weights are defined by

$$W_0^{\text{mean}} = \frac{\lambda}{n + \lambda} \quad (17a)$$

$$W_0^{\text{cov}} = \frac{\lambda}{n + \lambda} + (1 - \alpha^2 + \beta) \quad (17b)$$

$$W_i^{\text{mean}} = W_i^{\text{cov}} = \frac{1}{2(n + \lambda)}, \quad i = 1,\, 2,\, \ldots,\, 2n \quad (17c)$$

where β is used to incorporate prior knowledge of the distribution (a good starting guess is $\beta = 2$).

Two types of measurements are expected: latitude-longitude pairs, and lines of bearing (ψ). The measurement ellipsoid of the former is given in terms of cartesian position in the NED reference frame. The two measurement models are given by

$$\mathbf{h}_1 = \begin{bmatrix} \lambda \\ \phi \end{bmatrix} \quad (18)$$

$$h_2 = \psi = \tan^{-1}\left(\frac{y}{x}\right) \quad (19)$$

where x and y are the local NED positions [28].

The measurement vector $\tilde{\mathbf{y}}$ will either be equal to $\mathbf{h}_1$ or h_2, depending on the type of measurement. The Kalman update equations require the partial derivatives of these terms with respect to the states:

$$H_1 = \frac{\partial \mathbf{h}_1}{\partial \mathbf{x}} = \begin{bmatrix} 1 & 0 \\ 0 & 1 \end{bmatrix} \quad (20)$$

$$H_2 = \frac{\partial h_2}{\partial \mathbf{x}} \quad (21)$$

The calculation of the partial derivative of h_2 is not shown for brevity.

4 Trafficability

The trafficability matrix is a grid where local terrain traversability information is stored. This includes terrain slope, soil information, vegetation, weather conditions, etc. Each square contains information for a 90 meter by 90 meter area of land. This information is given by the variable v_i, which is a decimal value between 0 and 1. This corresponds to the fraction of maximum velocity that the vehicle can achieve in that grid location.

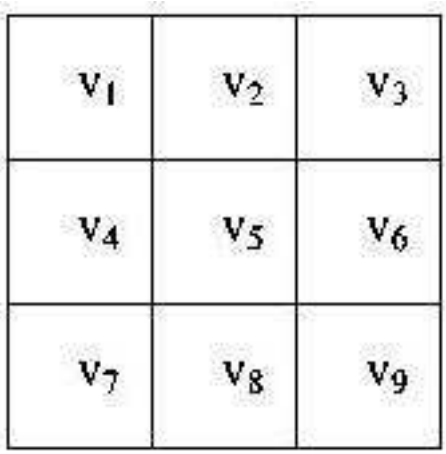

Figure 2: Velocity Constraint for Trafficability Matrix

This data will be used to deflect the direction of motion given by past state information. A generic representation of velocity constraint information in a trafficability matrix is shown in Fig. 2. The vehicle is assumed to be located in square 5 of the 3×3 grid. This results in the coefficient ν being given the value of v_5. The 3 by 3 grid will be continually re-centered about the vehicle as it moves throughout the region so that it is always located in square 5. A preferred direction based on the velocity constraint will be calculated based upon the equation

$$\hat{\mathbf{G}}_{tg} = \frac{\sum_j (v_j \hat{\mathbf{G}}_j)}{\| \sum_j (v_j \hat{\mathbf{G}}_j) \|} \tag{22}$$

where $j \, \epsilon \, J$ is a set of feasible directions. The unit vector $\hat{\mathbf{G}}_j$ points from the center of square 5 to the center of square j. It is assumed that a vehicle's velocity will not change its direction by more than ninety degrees between two consecutive time steps. Thus, cutoff lines perpendicular to the previous direction of motion will be used, extending from the center of square 5. An example is shown in Fig. 3. A square is assumed feasible if its centroid is contained within the feasible region. For this example, squares 1, 2, 4 and 7 are feasible and therefore included in set J. It should be noted that this method will always result in four feasible squares.

This technique for determining the cutoff was chosen because it is least expensive in terms of computational requirements. Another possible solution is to use the current estimated target position instead of the location of the center of square 5 for the above calculations. The unit vectors to the centers of other squares along with the tangent cutoff lines would then require more computational cost. This is demonstrated in Figs. 4(a) and 4(b), where a vehicle is close to the border of the central square. In both cases, the number of feasible squares to be used for direction determination differs from the previous standard of four. A possible advantage is that the set of feasible adjacent squares would be more accurate for cases when the vehicle is near the border of square 5.

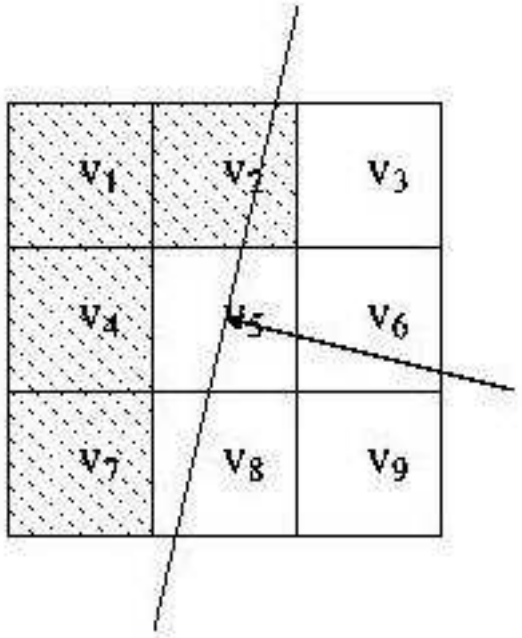

Figure 3: Cutoff for Velocity Based Direction Determination

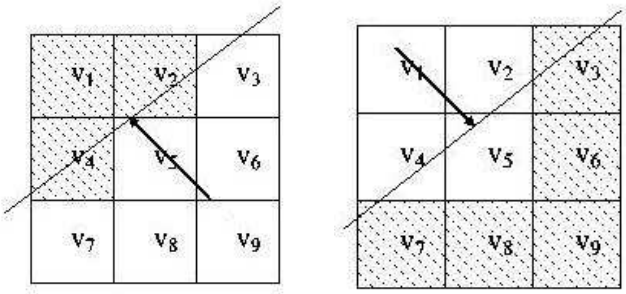

(a) Small Feasible Region (b) Large Feasible Region

Figure 4: Different Feasible Regions

The assumed direction of motion will be given by

$$\hat{\mathbf{G}}^{+} \;=\; \hat{\mathbf{G}}^{-} + \alpha_1 \hat{\mathbf{G}}_{tg} \tag{23}$$

where $\hat{\mathbf{G}}^{-}$ is the direction of motion at the previous time step, and α_1 is a weighting coefficient that is a function of v_j.

The proposed functional form for α_1 is based on the average difference in velocity constraint between the current location and the surrounding feasible locations.

$$\mu \;=\; \frac{\sum_j (v_j - v_5)}{\sum_j (1)} \tag{24}$$

The plot of α_1 is shown in Fig. 5. Since the goal is to use velocity information to slightly alter the assumed direction, the maximum magnitude of α_1 was chosen to be 0.5. Several cases can be discussed from this plot. First, consider the scenario where all feasible cells have the

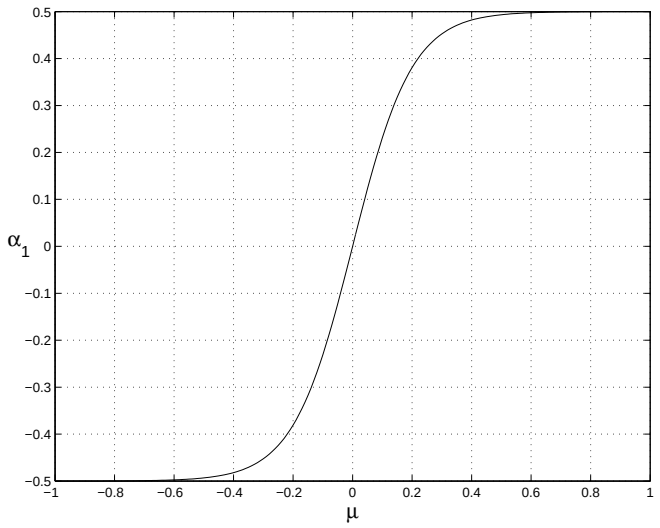

Figure 5: Proposed form for Coefficient α_1

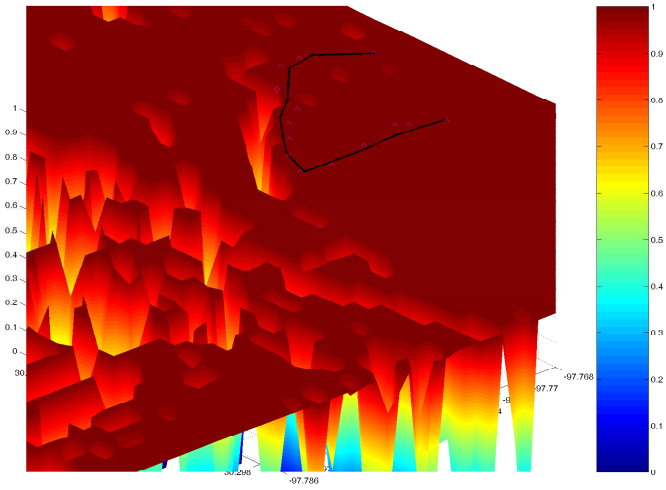

Figure 6: 3D Terrain with Trajectory

same velocity constraint coefficient as the current location. When that occurs, each of the cells is equally probable and should have no influence on the overall direction. From the plot, this scenario corresponds to $\mu = 0$, which yields $\alpha_1 = 0$. Another scenario is when the vehicle is facing impassable territory in all feasible directions (velocity coefficients of zero). This will result in a negative μ, corresponding to a negative α_1. This causes the assumed direction to be directed away from the impassable regions.

The case may also arise where goal information is present. Designate $\hat{\mathbf{G}}_{ob}$ as the unit vector pointing from the center of square 5 (or current estimated location if higher complexity is desired) to the location of the goal, and let d_{ob} be the distance between the two locations. The assumed direction can then be written as

$$\hat{\mathbf{G}}^{+} = \hat{\mathbf{G}}^{-} + \alpha_1 \hat{\mathbf{G}}_{tg} + \alpha_2 \hat{\mathbf{G}}_{ob} \tag{25}$$

where the positive coefficient α_2 is a function of d_{ob}. If goal information is withdrawn for a given target, α_2 is set to zero, and Eq. (23) is recovered. A proposed form for α_2 is

$$\alpha_2(r,s) = \frac{1}{(1+\frac{d_{ob}}{90})^n} \tag{26}$$

where n is a positive user-defined coefficient. The "1" in the denominator ensures that a singularity will not occur if the target is located within a region containing a goal. Dividing the distance-to-object by 90 normalizes that value with respect to the grid size. When the goal is far away, this will have a small effect on the overall direction. As the target approaches the goal, the influence of that goal will increase more rapidly. The coefficient n will be best determined by testing after real traversability and goal information have been provided. At this time, a value of $n = 1$ is recommended.

5 Results

Based on trafficability data provided by Overwatch Systems for the the Austin, Texas area, a test case was generated to illustrate the performance of the trafficability based filter. The trafficability data ranges from 0 to 1, where 0 for any region corresponds to infeasibility of the vehicle traversing that region and a 1 corresponds to no constraints on the motion of the vehicle. The trafficability data is provided for a grid of cells where each cell corresponds to a 90 m by 90 m area. A test case which corresponds to a vehicle traveling towards a gully and subsequently making a sharp right turn and following the gully as shown in Figure 6, is created. The black line is the true path of the vehicle and the diamonds represent the periodic measurements of the vehicle. The additive Gaussian noise is the reason why the magenta diamonds do not lie on the black line. A sampling time of 10 seconds or a sampling rate of 6 measurements per minute, is selected for sampling the position of the vehicle.

An Unscented filter (UF) is used to predict the motion of the ground vehicle and the resulting trajectory is illustrated by the blue line in Figure 7. The UF filter does not exploit knowledge of the trafficability and therefore, as the vehicle approaches the gulley, the velocity vector of the vehicle prior to the sharp turn, predicts the motion of the vehicle to lie in the gulley. The following measurements coax the UFs trajectory out of the gulley. In contrast, the UF filter which exploits the trafficability data to nudge the velocity vector of the UF is illustrated by the green line. The benefit of knowledge of the trafficability is illustrated by the trajectory which avoids motion in the gulley.

Figure 8 illustrates the benefit of using the trafficability data to modify the velocity vector in a planar view of the terrain. The colorbar on the right which ranges for a numerical value of 0 to 1 provide the context for the trafficability of the vehicle. The x and y axes represent the latitude and longitude respectively with units of degrees.

This example illustrates the potential of using the traf-

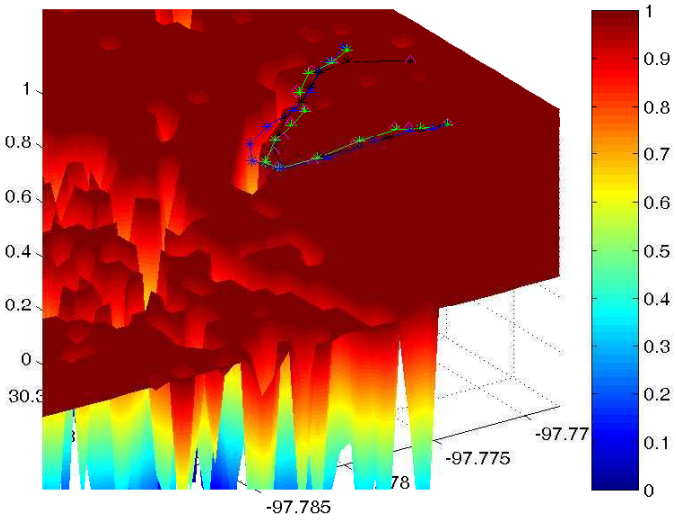

Figure 7: 3D Terrain with Filter Results

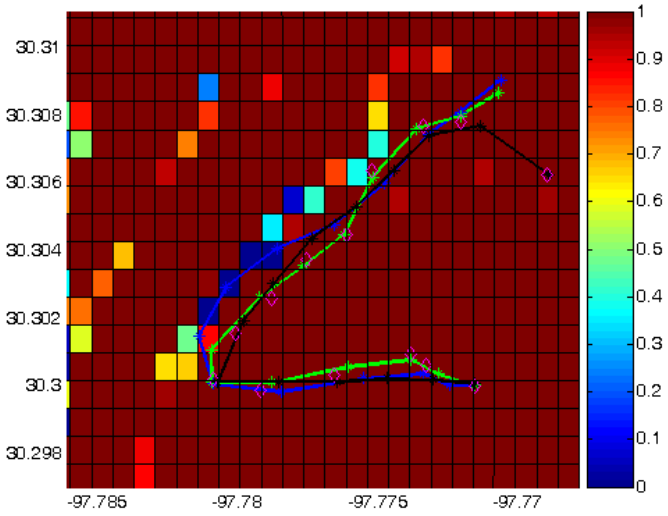

Figure 8: 2D Terrain with Filter Results

ficability data to enhance the performance of traditional filtering approaches. It should be pointed out that since the proposed approach to nudge the velocity vector is ad-hoc, with many tuning parameters, numerical studies are necessary for the appropriate selection of the tuning parameters to optimize the performance of the proposed filter.

6 Conclusions

A new tracking filter was developed that incorporates trafficability information. This information was used to deflect the direction of motion given by past state information. A preferred direction based on the velocity constraint was calculated, which assumed that a vehicles velocity will not change its direction by more than ninety degrees between two consecutive time steps. Goal information has also been introduced into the deflection vector. Simulation results indicated that the new filter based on trafficability clearly outperforms the traditional approach without trafficability information.

Acknowledgment

The first three authors were supported through a grant by Overwatch Systems. These authors greatly appreciate this support.

References

[1] K. Kastella and C. Kreucher, "Multiple Model Nonlinear Filtering for Low Signal Ground Target Applications," *IEEE Transactions on Aerospace and Electronic Systems*, Vol. 41, No. 2, Apr. 2005, pp. 549–564.

[2] H. Blom and Y. Bar-Shalom, "The Interacting Multiple Model Algorithm for Systems with Markovian Switching Coefficients," *IEEE Transactions on Automatic Control*, Vol. 33, No. 8, Aug. 1988, pp. 780–783.

[3] W. Li and Y. Bar-Shalom, "Performance Prediction of the Interacting Multiple Model Algorithm," *IEEE Transactions on Aerospace and Electronic Systems*, Vol. 29, No. 3, Jul. 1993, pp. 755–771.

[4] L. Johnston and V. Krishnamurthy, "An Improvement to the Interacting Multiple Model (IMM) Algorithm," *IEEE Transactions on Signal Processing*, Vol. 49, No. 12, Dec. 2001, pp. 2909–2923.

[5] Y. Boers and J. Driessen, "Interacting Multiple Model Particle Filter," *Radar, Sonar and Navigation, IEE Proceedings*, Vol. 150, No. 5, Oct. 2003, pp. 344–349.

[6] T. Kirubarajan, Y. Bar-Shalom, and K. Pattipati, "Topography Based vs. IMM Estimator for Large Scale Ground Target Tracking," *IEEE Colloquium on Target Tracking: Algorithms and Applications*, 1999, pp. 11/1–11/4.

[7] J. Layne and U. Piyasena, "Adaptive Interacting Multiple Model Tracking of Maneuvering Targets," *Digital Avionics Conference*, Oct. 1997.

[8] H. Yan, G. Zhi-Jiang, and J. Jing-ping, "Design of the Adaptive Interacting Multiple Model Algorithm," *American Control Conference*, 2002, pp. 1538–1542.

[9] A. Munir and D. Atherton, "Maneuvering Target Tracking Using and Adaptive Interacting Multiple Model Algorithm," *Proceedings of the American Control Conference*, June 1994.

[10] J. Gustafson and P. Maybeck, "Control of a Large Flexible Space Structure with Moving-Bank Multiple Model Adaptive Algorithms," *Proceedings of the*

31^{st} *Conference on Decision and Control*, December 1992, pp. 1273–1278.

[11] P. Maybeck and K. Hentz, "Investigation of Moving-Bank Multiple Model Adaptive Algorithms," *AIAA Journal of Guidance, Navigation, and Control*, Vol. 10, No. 1, 1987, pp. 1273–1278.

[12] M. Efe and D. Atherton, "Maneuvering Target Tracking with an Adaptive Kalman Filter," *IEEE Conference on Decision and Control*, Dec. 1998, pp. 737–742.

[13] O. Payne and A. Marrs, "An Unscented Particle Filter for GMTI Tracking," *Proceedings of the 2004 IEEE Aerospace Conference*, Vol. 3, 2004, pp. 1869–1875.

[14] M. Hernandez, "Performance Bounds for GMTI Tracking," *Proceedings of the Sixth International Conference of Information Fusion*, Vol. 1, 2003, pp. 406–413.

[15] S. Arulampalam, N. Gordon, M. Orton, and B. Ristic, "A Variable Structure Multiple Model Particle Filter for GMTI Tracking," *Fifth International Conference on Information Fusion*, Vol. 2, 2002, pp. 927–934.

[16] Y. Cheng and T. Singh, "Efficient Particle Filtering for Road-Constrained Target tracking," *Eighth International Conference on Information Fusion*, Jul. 25 - 29 2005.

[17] X. Li and Y. Bar-Shalom, "Multiple Model Estimation with Variable Structure," *IEEE Transactions on Automatic Control*, Vol. 41, No. 4, Apr. 1996, pp. 478–493.

[18] T. Kirubarajan and Y. Bar-Shalom, "Tracking Evasive Move-Stop-Move Targets with a GMTI Radar Using a VS-IMM Estimator," *IEEE Transactions on Aerospace and Electronic Systems*, Vol. 39, No. 3, Jul. 2003, pp. 1098–1103.

[19] T. Kirubarajan, Y. Bar-Shalom, K. Pattipati, and I. Kadar, "Ground Target Tracking with Variable Structure IMM Estimator," *IEEE Transactions on Aerospace and Electronic Systems*, Vol. 36, No. 1, Jan. 2000, pp. 26–46.

[20] G. Kravaritis and B. Mulgrew, "Ground Tracking Using a Variable Structure Multiple Model Particle Filter with Varying Number of Particles," *IEEE International Radar Conference*, 2005, pp. 837–841.

[21] R. Enders, "Fundamentals of On-Road Tracking," *SPIE Conference on Aquisition, Tracking and Pointing*, Apr. 1999.

[22] P. Nougues and D. Brown, "We Know Where You Are Going: Tracking Objects in Terrain," *IMA Journal of Mathematics Applied in Business & Industry*, Vol. 8, 1997, pp. 39–58.

[23] C. Yang, M. Bakich, and E. Blasch, "Nonlinear Constrained Tracking of Targets on Roads," *Eigth International Conference on Information Fusion*, 2005.

[24] D. Tenne, B. Pitman, T. Singh, and J. Llinas, "Velocity Field Based Tracking of Ground Vehicles," *RTO-SET-059: Symposium on "Target Tracking and Sensor Data Fusion for Military Observation Systems"*, Oct. 15-17 2003.

[25] M. Mallick, T. Kirubarajan, and S. Arulampalam, "Out-of-Sequence Measurement Processing for Tracking Ground Target Using Particle Filters," *IEEE Aerospace Conference*, Vol. 4, 2002, pp. 1809–1818.

[26] B. Kim and J. Lee, "IMM Algorithm Based on the Analytic Solution of Steady State Kalman Filter for Radar Target Tracking," *IEEE International Radar Conference*, 2005, pp. 757–7622.

[27] D. Reid and R. Bryson, "A Non-Gaussian Filter for Tracking Targets Moving Over Terrain," *Asilomar Conference on Circuits, Systems, and Computers*, 1978.

[28] J. Farrell and M. Barth, *The Global Positioning System and Inertial Navigation*, McGraw-Hill, New York, NY, 1998.

[29] B. Hofmann-Wellenhof, H. Lichtenegger, and J. Collins, *GPS: Theory and Practice*, Springer Wien, New York, NY, 2001.

[30] J. Crassidis and J. Junkins, *Optimal Estimal of Dynamic Systems*, CRC Press, Boca Raton, FL, 2004.

[31] E. Wan and R. van der Merwe, *The Unscented Kalman Filter*, edited by S. Haykin, chap. 7, John Wiley & Sons, New York, NY, 2001.